

Computer vision-based framework for extracting tectonic lineaments from optical remote sensing data

Ehsan Farahbakhsh, Rohitash Chandra, Hugo K. H. Olierook, Richard Scalzo, Chris Clark, Steven M. Reddy & R. Dietmar Müller

To cite this article: Ehsan Farahbakhsh, Rohitash Chandra, Hugo K. H. Olierook, Richard Scalzo, Chris Clark, Steven M. Reddy & R. Dietmar Müller (2019): Computer vision-based framework for extracting tectonic lineaments from optical remote sensing data, International Journal of Remote Sensing, DOI: [10.1080/01431161.2019.1674462](https://doi.org/10.1080/01431161.2019.1674462)

To link to this article: <https://doi.org/10.1080/01431161.2019.1674462>



Published online: 11 Oct 2019.



Submit your article to this journal



Article views: 42



View related articles



View Crossmark data



Computer vision-based framework for extracting tectonic lineaments from optical remote sensing data

Ehsan Farahbakhsh^{a,b,c}, Rohitash Chandra^{a,b}, Hugo K. H. Olierook^d, Richard Scalzo^c, Chris Clark^d, Steven M. Reddy^d and R. Dietmar Müller^a

^aEarthByte Group, School of Geosciences, University of Sydney, Sydney, Australia; ^bCentre for Translational Data Science, University of Sydney, Sydney, Australia; ^cDepartment of Mining and Metallurgical Engineering, Amirkabir University of Technology (Tehran Polytechnic), Tehran, Iran; ^dSchool of Earth and Planetary Sciences, Curtin University, Perth, Australia

ABSTRACT

The extraction of tectonic lineaments from digital satellite data is a fundamental application in remote sensing. The location of tectonic lineaments such as faults and dykes are of interest for a range of applications, particularly because of their association with hydrothermal mineralization. Although a wide range of applications have utilized computer vision techniques, a standard workflow for application of these techniques to tectonic lineament extraction is lacking. We present a framework for extracting tectonic lineaments using computer vision techniques. The proposed framework is a combination of edge detection and line extraction algorithms for extracting tectonic lineaments using optical remote sensing data. It features ancillary computer vision techniques for reducing data dimensionality, removing noise and enhancing the expression of lineaments. The efficiency of two convolutional filters are compared in terms of enhancing the lineaments. We test the proposed framework on Landsat 8 data of a mineral-rich portion of the Gascoyne Province in Western Australia. To validate the results, the extracted lineaments are compared to geologically mapped structures by the Geological Survey of Western Australia (GSWA). The results show that the best correlation between our extracted tectonic lineaments and the GSWA tectonic lineament map is achieved by applying a minimum noise fraction transformation and a Laplacian filter. Application of a directional filter shows a strong correlation with known sites of hydrothermal mineralization. Hence, our method using either filter can be used for mineral prospectivity mapping in other regions where faults are exposed and observable in optical remote sensing data.

ARTICLE HISTORY

Received 20 April 2019

Accepted 6 August 2019

1. Introduction

Digital satellite data with different spatial and spectral resolution are available for almost every locality on the Earth's land surface (El Janati et al. 2014; Thenkabail et al. 2015; van der Werff and van der Meer 2016; Hewson et al. 2017; Dos Reis Salles et al. 2017). This enables the procurement of detailed information from surficial features and processes at

CONTACT Ehsan Farahbakhsh e.farahbakhsh@sydney.edu.au EarthByte Group, School of Geosciences, University of Sydney, Sydney, Australia

© 2019 Informa UK Limited, trading as Taylor & Francis Group

different scales. Linear features are considered as one of the most important surficial features in different fields of study (Hao et al. 2007; He et al. 2008; Pirasteh et al. 2013). A linear feature is a two-dimensional, straight or slightly curved line, linear pattern or alignment of discontinuous patterns evident in an image, photo or map (Wang 1993). Linear features represent the expression of some degree of linearity of a single or diverse grouping of both natural and cultural features (Wang 1993; Simonett and Ulaby 1983). Their specific physiographic characteristics make it possible to detect them due to the tonal change in digital satellite data (Hashim et al. 2013). Natural features include any linear features formed by natural processes such as drainage networks, tectonic or geomorphological lineaments and vegetation alignments. Cultural features comprise man-made features such as road networks, railroads, and electrical or telecommunications networks (Wang 1993).

The identification of linear features in remote sensing imagery can be complex since their spatial and spectral characteristics vary along their extent (Wang 1993). A variety of techniques have emerged for extracting linear features from digital satellite data for different applications such as seismic and earthquake studies (Singh et al. 2001; Singh and Singh 2005; Nath, Niu, and Acharjee 2017; Nath, Niu, and Mitra 2019), detecting road networks (Valero et al. 2010; Singh and Garg 2013), drainage networks (Martinez et al. 2009; Paiva, Durand, and Hossain 2015), and tectonic lineaments (Hashim et al. 2013; Marghany and Hashim 2010; Beiranvand Pour and Hashim 2015). Tectonic lineaments are an expression of the underlying geological structure and include faults, dykes, shear zones and folds. Linear to curvilinear faults, dykes and shear zones are of particular interest in assisting mineral prospecting because of their association with hydrothermal mineralization (Beiranvand Pour and Hashim 2015; Beiranvand; Pour et al. 2016; Manuel et al. 2017) but their applications also extend to hydrogeological (Bhuiyan 2015; Dasho et al. 2017; Akinluyi, Olorunfemi, and Bayowa 2018; Takorabt et al. 2018) and tectonic studies (Arian and Nouri 2015; Daryani, Arian, and Omran 2015; Masoud and Koike 2017). Faults, dykes and shear zones may be used to delineate major structural units, analyse of structural deformation patterns, and identify geological boundaries and uncover mineral deposits (Glasser and Ghiglione 2009; Saadi, Aboud, and Watanabe 2009; Raharimahefa and Kusky 2009; Ramli et al. 2010; Beiranvand Pour and Hashim 2014). Mineral deposits are commonly clustered around specific positions along deep crustal structures, which often have surface expressions in the absence of sedimentary or regolith cover (Lund et al. 2011; Hein et al. 2013). Understanding the structural mechanisms for hydrothermal ore deposits along deep crustal discontinuities are pivotal in terms of economic considerations. Faults usually act as conduits for mineralizing fluids and hosts to the ore bodies (Petrov et al. 2015). Some researchers posit that fault bends are the primary control for ore clusters (Cox 1999; Allibone et al. 2002), while others believe that fault intersections are most important (Craw 2000; Allibone et al. 2002; Lu, Liu, and Xu 2016). Although both cases are sometimes important in formation of hydrothermal ore deposits. Irrespective of the mechanism, detecting tectonic lineaments can help link surface lineament expressions to deep-seated structural discontinuities, which ultimately aids in mineral prospectivity mapping.

Although manual interpretation is effective at identifying tectonic lineaments (Saadi and Watanabe 2008; Saad and Mohammed 2011), computer vision techniques are required to make this process efficient. Computer vision is an interdisciplinary field that

employs a wide range of algorithms for gaining a high-level understanding from digital images or videos. In other words, it seeks to automate tasks akin to what the human visual system can accomplish (Ballard and Brown 1982; Sonka, Hlavac, and Boyle 2014). Computer vision is concerned with automatic extraction, analysis and understanding of useful information from a single image or a sequence of images. It involves the development of a theoretical and algorithmic basis to achieve automatic visual understanding (Szeliski 2010). Some of the applications of computer vision include systems for automatic inspection, detecting events, modelling objects and organizing information (Szeliski 2010). In the geosciences, computer vision has diverse applications including surface modelling (James and Robson 2012), rock type classification (Patel and Chatterjee 2016), motion analysis (Gutierrez and Long 2002), edge detection and extracting linear features from digital imagery (Cross 1988).

The use of computer vision and digital satellite images to map tectonic lineaments has been particularly useful in regional scale studies that are inaccessible, unsafe or costly to navigate (Karnieli et al. 1996; Shahzad and Gloaguen 2011). The lineament mapping is traditionally based on a visual or manual photointerpretation. Manual digitizing of lineaments is subjective, time consuming and expensive (Rahnama and Gloaguen 2014a). Therefore, a reliable and standard framework consisting of available computer vision techniques is needed. This framework must be able to work with different satellite images representing different spatial and spectral resolutions. The success of tectonic lineament extraction procedures depends on the sequence of applied techniques, and the reliability and accuracy of the edge detection and line extraction mechanisms (Karantzalos and Argialas 2006). Selection of computer vision techniques, appropriate edge detection methods and line extraction methods are pivotal in extracting tectonic linear features because they exert significant influence on the accuracy of the final results.

In this study, we present a framework for detecting tectonic lineaments using computer vision techniques that include edge detection and line extraction methods. To demonstrate the validity of this framework, we use Landsat 8 satellite data and shuttle radar topography mission (SRTM) digital elevation models for extracting tectonic lineaments of the Yinnetharra 1:100,000 scale map sheet located in the Capricorn Orogen, Western Australia (Figure 1). Satellite data are subjected to dimensionality reduction, noise removal and lineament enhancement prior to edge detection and line extraction algorithms. The extracted tectonic lineaments are compared to geological mapping by the Geological Survey of Western Australia (GSWA) (S. P. Johnson et al. 2012). We also investigate the correlation between extracted tectonic lineaments and known mineral occurrences in the study area. The final product of our workflow is an efficient evidential data layer for detecting hydrothermal mineral deposits.

2. Geological setting of the study area

The Yinnetharra 1:100,000 scale map sheet is situated within the western portion of the Capricorn Orogen, known as the Gascoyne Province (Figure 1) (Johnson et al. 2013). The Gascoyne Province, and the wider Capricorn Orogen, record the protracted amalgamation of the West Australian Craton and subsequent intracontinental tectono-thermal activity. Two main events have been found to contribute to forming the West Australian Craton. First, the Ophthalmia Orogeny aged about 2195–2145 million years (Ma) sutured the

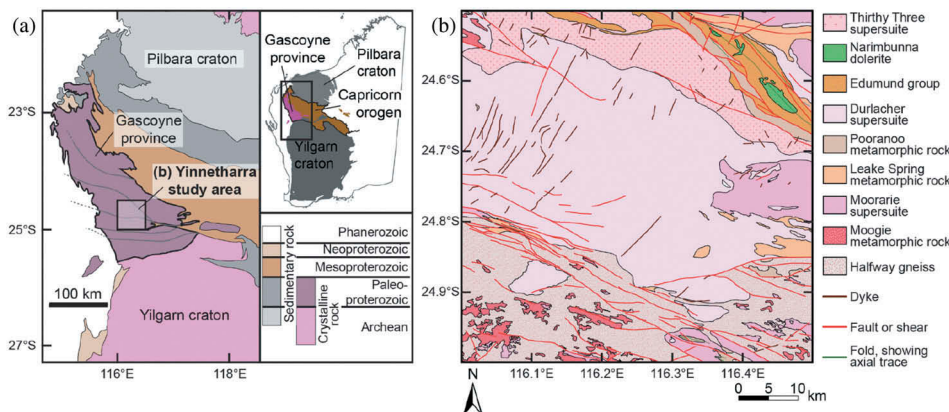


Figure 1. (a) Map of the capricorn orogen showing the tectonic units and study area (modified from Olierook et al. 2018); (b) simplified geological map of Yinnetharra 1:100,000 scale map sheet (after S. P. Johnson et al. 2012).

Glenburgh Terrane (comprised of the Halfway Gneiss) to the Pilbara Craton (Rasmussen, Fletcher, and Sheppard 2005; Krapež et al. 2017). The Ophthalmia Orogeny was associated with the deposition of the Moogie Metamorphics, which was deposited into a foreland basin that formed as a response to the Glenburgh–Pilbara collision (Johnson et al. 2013). Second, the Glenburgh Orogeny aged about 2005–1950 Ma amalgamated the combined Pilbara Craton–Glenburgh Terrane with the Yilgarn Craton to form the West Australian Craton (Johnson et al. 2013; Olierook et al. 2018). The Glenburgh Orogeny was associated with two major Andean-type granitoid formations, the Dalgarinka and Bertibubba Supersuites, and several subduction-related basins (Olierook et al. 2018; Johnson et al. 2011). After unification, the Capricorn Orogen experienced at least five intracontinental tectono-magmatic events, each decreasing in severity of tectonic character and magmatism (Johnson et al. 2017). The first two events, the 1830–1780 Ma Capricorn Orogeny and 1680–1620 Ma Mangaroon Orogeny, were both associated with significant granitoid magmatism of the Moarie and Durlacher Supersuites, respectively (Sheppard, Occhipinti, and Nelson 2005; Sheppard et al. 2010; Piechocka et al. 2017). Later events were predominantly amagmatic but were still associated with up to amphibolite-facies metamorphism and hydrothermal activity (Sheppard et al. 2007; Korhonen et al. 2017; Piechocka et al. 2018; Olierook et al. 2019a, 2019b).

Both suturing and intracontinental tectonic events have developed a pervasive east–west striking structural fabric in the Gascoyne Province that has compartmentalized the region into several geological ‘zones’ that share tectonic characteristics (Sheppard et al. 2010). In the south, zone and formation boundaries trend southwest–northeast (SW–NE) whereas major structures are oriented northwest–southeast (NW–SE) in the north, yielding a wedge-shaped geometry for the western margin of the Capricorn Orogen (Figure 1). Compared to the rest of the Capricorn Orogen, the Gascoyne Province is relatively well exposed, but there are still significant regions of recent cover that hamper mineral exploration. Known precious and base metal mineralization predominantly occur along and are associated with structural discontinuities (Johnson et al. 2013). A crucial aspect to the mineralization potential in the Capricorn Orogen is the repeated reactivation of major

structures over a billion years, which allows mineralization to be upgraded to economic scales (Pirajno 2004; Zi et al. 2015).

3. Computer vision techniques

3.1. Dimension reduction

Dimension reduction is a machine learning method that reduces a set of random variables by obtaining a set of principal variables (Zhang and Kwok 2010; Lafon and Lee 2006). Dimension reduction techniques can be divided into transformation methods (feature extraction) and feature selection methods (Huang, Zhang, and Li 2007). The transformation methods can be further characterized as principal component analysis (PCA), independent component analysis (ICA) and minimum noise fraction (MNF). They separate significant and insignificant parts of the data in addition to reducing data dimensionality. In remote sensing applications, dimension reduction techniques are initially used to compress available information stored in multiple bands into a few bands. In other words, a multispectral image is converted into a greyscale image while preserving maximum information. This technique can also be applied for different purposes such as statistical analysis and classification (Lafon and Lee 2006). In the proposed framework for extracting tectonic lineaments, we obtained satisfactory results using minimum noise fraction and further details of this method are presented in the following.

3.1.1. Minimum noise fraction

Minimum noise fraction is similar to the PCA transform and is an effective technique for reducing a large multi-dimensional data set such as hyperspectral images into a fewer number of components that contain the majority of information (Green et al. 1988). Unlike a PCA transform, the resulting axes or components are not necessarily orthogonal, but are ordered by decreasing signal-to-noise ratio in terms of image quality (Harris et al. 2005). Moreover, MNF is applied to isolate noise from signal in a data set and to determine inherent dimensionality of an image. Minimum noise fraction is also able to reduce computational requirements for subsequent processing (Boardman and Kruse 1994).

There can be as many components as there are input bands; however, each component, starting from the first, describes less and less of the overall variance of the data set. Typically, only a small number of components are required to describe most of the information for the entire data set. The contribution of each component to the overall information in a multivariate data set (i.e. multispectral or hyperspectral imagery) is measured by an eigenvalue. A larger eigenvalue indicates that a component contains more information from the data set. The contribution of each band to each component is measured by an eigenvector, which can be interpreted akin to a correlation coefficient.

3.2. Image enhancement

The image enhancement techniques are applied to increase the quality of image interpretation based on enhancing edges of features prior to their detection and extraction. Different types of filtering such as adaptive and convolutional filtering are part of this suite of techniques.

Adaptive filtering uses the standard deviation of those pixels within a local box surrounding each pixel to calculate a new pixel value. Typically, the original pixel value is replaced with a new value calculated based on the surrounding valid pixels which satisfy the standard deviation criteria (Crow and Reichle 2008). The adaptive filters are particularly adept at preserving image sharpness and detail while suppressing noise. Lee filter is an adaptive filter which is used to smooth noisy and speckled data that have an intensity related to the image scene and that also have an additive and/or multiplicative component (Lee 1980).

Convolutional filters yield images in which brightness value at a given pixel is a function of weighted average of surrounding pixels' brightness. Convolution of a user-selected kernel with the image array returns a new, spatially filtered image. Different kernel size and values produce different types of filters. Standard convolutional filters include high pass, low pass, Laplacian, directional, median, Sobel and Roberts (Richards 2013; Haralick, Sternberg, and Zhuang 1987).

In the proposed framework for extracting tectonic lineaments, we use median filter and compare directional and Laplacian filters. A median filter is applied for smoothing an image and removing speckling noise, while preserving edges larger than the kernel dimensions (Chan, Ho, and Nikolova 2005). This low frequency filter replaces each centre pixel with the median value within the neighbourhood specified by the filter size (Haralick, Sternberg, and Zhuang 1987). A directional filter is a first derivative edge enhancement filter that selectively enhances image features having specific direction components (gradients) (Zhang and Xiaolin 2006). The sum of the directional filter kernel elements is zero. The result is that areas with uniform pixel values are zeroed in the output image, while those that are variable are presented as bright edges. A Laplacian filter is a second derivative edge enhancement filter that operates without regard to edge direction (Lee and Park 1990). Laplacian filtering emphasizes maximum values within the image using a kernel with a high central value typically surrounded by negative weights in north–south (N–S) and east–west (E–W) directions and zero values at the kernel corners (Haralick, Sternberg, and Zhuang 1987).

3.3. Lineament extraction

Linear features can be divided into two major subclasses that include edges and lines on a digital greyscale image. An edge in an image is an abrupt discontinuity in image brightness, which may result from surface boundaries, shadow boundaries or changes in surface reflectance. A line in an image is a digital valley or ridge of image brightness (Wang 1993). Lines may be formed, for example, by roads, rivers, and vegetation alignments, as well as by geological faults and joints. Lineament extraction methods can be conducted via manual photointerpretation by an expert or (semi-)automatic detection using computer vision techniques (Vassilas et al. 2002). The automatic methods have resulted in a more efficient lineament extraction process (Tripathi, Gokhale, and Siddiqui 2000; Masoud and Koike 2006, 2011). A lineament extraction process comprises two main steps, namely edge detection and line extraction.

3.3.1. Edge detection

In general, automatic lineament extraction methods are based on edge detection techniques that enhance the pixels at the edges on an image, instead of directly extracting

edge contours. An edge in an image is defined as a boundary or contour at which a significant change occurs in some physical aspect of the image. Linear operators can detect edges through the use of masks that represent the ideal edge steps in various directions (Ali and Clausi 2001). They can detect lines and curves in much the same way. Traditional edge detectors were based on a rather small neighbourhood, which only examined each pixel's nearest neighbour (Cyganek 2003; Awad and Man 2008). This may work well but due to the size of the neighbourhood that is being examined, there are limitations to the accuracy of the final edge. These local neighbourhoods will only detect local discontinuities, and it is possible that this may cause false edges to be extracted. A more powerful approach is to use a set of first or second difference operators based on neighbourhoods having a range of sizes and combine their outputs, so that discontinuities can be detected at various scales (Ballard and Brown 1982).

Laplace, zero-crossing and gradient operators are the primary edge detection techniques (Ali and Clausi 2001; Patel et al. 2011). Laplace operators compute some quantity related to the divergence of the intensity surface gradient of the greyscale images. Zero-crossing operators determine whether or not the digital Laplacian or the estimated second direction derivative has a zero-crossing within the pixel (Ali and Clausi 2001). Gradient operators compute some quantity related to the magnitude of the slope of the greyscale image wherein the image pixel values are noisy discretized samples. The major drawback of such an operator is the fact that determining the actual location of the edge and slope turnover point is difficult (Ali and Clausi 2001). The frequency and connectivity of the extracted edges by common edge detection methods are strongly affected by the type and spatial resolution of the source datasets, signal-to-noise ratio and the parameters of the edge detection methods (Zhang et al. 2006). In other words, results of most edge detection methods involve fragmented edges and should be ultimately interpreted visually.

An alternative technique is known as Canny edge detection, which is based on computing the squared gradient magnitude (Canny 1986). Local maxima of the gradient magnitude that are above some threshold are identified as the edges. The advantages of the Canny edge operator are deriving an optimal operator in the sense that minimizes the probability of multiply detecting an edge, minimizing the probability of failing to detect an edge, and minimizing the distance of the reported edge from the true edge. There is a trade-off between detection and localization; the more accurate the detector the less accurate the localization and vice-versa (Ali and Clausi 2001). An objective function has been designed to achieve some optimization constraints including maximizing the signal-to-noise ratio to give perfect detection which favours the marking of true positives; achieving perfect localization to accurately mark the edges; minimizing the number of responses to a single edge which favours the identification of true negatives and prevents marking non-edges (Ali and Clausi 2001).

3.3.2. Line extraction

After edge detection, additional processing must be performed in order to remove false edge responses and to link gaps between edges, ultimately turning isolated edges into lines. This processing turns the linearization of the edge pixels into continuous contours, using certain criteria such as closeness or some specific geometric property such as the degree of curvature (Ghita and Whelan 2002).

Edge-linking methods can be classified into two categories, namely local and global processing methods (Rahnama and Gloaguen 2014b). In local processing methods such as pixel connectivity-edge linking and gradient-based methods, edge pixels are grouped to form edges by considering each pixel's relationship to any neighbouring edge pixels (Ghita and Whelan 2002). This method is suitable to link edge pixels in situations where the shape of the edge (e.g. tectonic lineaments) is unknown. The pixel connectivity-edge linking algorithms have been widely used in applications which involve extraction of continuous line segments (Hashim et al. 2013). The global processing methods such as the Hough transform use all edge pixels. Pixels displaying similarities such as same edge geometry are used to find the best fit of a known shape. The global methods do not need to connect the edge pixels. However, these methods may miss small pieces of edges or noise pixels may wrongly be handled as edge segments (Yang, Sam Ge, and He 2011). The Hough transform is a well-known technique which tolerates noise and discontinuities in an image but it has limitations such as high computing time, unwieldy memory requirements and limited capability in preserving edge pixel connectivity (Hashim et al. 2013).

4. Materials and methods

4.1. Landsat 8 satellite data

The Landsat 8 satellite carries two instruments including the operational land imager (OLI) and thermal infrared sensor (TIRS). The OLI comprises nine spectral bands with a spatial resolution of 30 m for bands 1 to 7 and 9. The resolution for band 8 (panchromatic) is 15 m. The TIRS provides two thermal bands 10 and 11 that provide more accurate surface temperatures but are less useful for geological purposes (Irons, Dwyer, and Barsi 2012; Loveland and Dwyer 2012). These sensors both provide improved signal-to-noise radiometric performance quantized over a 12 bit dynamic range that enables better characterization of land cover state and condition compared to other Landsat satellites (Reuter et al. 2010). Moreover, geological features and the geomorphological framework are more readily distinguished.

The high-quality cloud-free Landsat 8 OLI level 2 data product (surface reflectance) is used in this study and was obtained from United States Geological Survey EarthExplorer system (US Geological Survey 2019). The considered scene was acquired on 13 February 2018. The scene was pre-georeferenced to Universal Transverse Mercator (UTM) zone 50 south projection with the World Geodetic System (WGS) 84 datum, but all the outputs of this study are provided in the Geocentric Datum of Australia (GDA) 94. Bands 1 and 9 are not used in this study, because they have been designed for retrieving atmospheric aerosol properties and detecting cirrus cloud, respectively (Adiri et al. 2016).

4.2. Structural geological maps

Structural geological maps represent the expression of underlying geological structures exposed at the Earth's surface (Lisle 2003). Structural analysis involves the description of the structural geometry of a deformed field area, kinematic analysis and dynamic analysis (Lageson 2009). Descriptive structural analysis is obtained through detailed field mapping, yielding positions, orientations and lengths of linear structures, including faults,

dykes and fold axes. No geological map is ever complete but mapping by the GSWA at a scale of 1:100,000 (Johnson et al. 2012) is an appropriate benchmark for assessing the validity of our final workflow results.

4.3. Computer vision-based framework for semi-automated extraction of tectonic lineaments

A detailed computer vision-based framework for semi-automatic extraction of tectonic lineaments from optical remote sensing data is presented in Figure 2. This framework starts with acquiring satellite images (Figure 2(a)). According to the level of satellite images, radiometric and geometric corrections are applied (Figure 2(b)). To transform satellite images from multiple bands into a greyscale (single-band) image, three dimension reduction techniques (PCA, ICA and MNF) are suggested (Figure 2(c)). In this study, we used the MNF due to obtaining better results compared to other techniques (Appendix A). After image transformation, Lee and median filters (Figure 2(d,e)) are applied respectively to the output component of the dimension reduction technique with the highest eigenvalue. To enhance edges, directional and Laplacian filters (Figure 2(f)) are subsequently applied on greyscale images using ENVI (Environment for Visualizing Images) 5.3 software package. The directional filter is applied using a 3×3 kernel in four directions with azimuths of 0° , 45° , 90° and 135° . Using these azimuths, the directional filter visually enhances the edges striking N–S, NE–SW, E–W and NW–SE, respectively. The Laplacian filter uses a 3×3 kernel with a value of 4 for the centre pixel and values of –1 for the N–S and E–W pixels.

Edge detection is performed using a Canny edge detector applied on the final greyscale image (Figure 2(g)). Canny edge detection is preferred over Laplace, zero-crossing or gradient operators because it is resistant to a noisy environment and signals can be enhanced with respect to the noise ratio by a non-maxima suppression method which results in one pixel wide ridges as the output. Lines are then extracted from the binary image produced by the Canny edge detection process using pixel connectivity-edge linking (Figure 2(h)). Pixel connectivity-edge linking is preferred over Hough transform or gradient based methods because all pixels identified as linear edge pixels are maintained (Guru, Shekar, and Nagabhushan 2004; Vučinić, Trpovski, and Šćepan. 2010).

The edge detection and lineament extraction processes rely on setting six different thresholds by the user utilizing PCI Geomatica 2016 software package, including filter radius, edge gradient, curve length, line fitting error, angular difference and linking distance (Figure 2(j); Table 1). Filter radius and edge gradient threshold are effective for the edge detection and the other thresholds are applied for the line extraction. Several combinations of the thresholds within the proposed ranges in Table 1 were evaluated and various validation criteria as well as the ground truth were applied to reach the optimum values which gave a satisfactory result. The Canny edge detection and pixel connectivity-edge linking methods are applied separately on every four output images after implementing directional filter (Figure 4(a,d)) for extracting the lineaments. The extracted lineaments from each image are combined and a comprehensive lineament map which covers major directions is generated.

The filter radius is initially used to determine the number of pixels to be considered around each pixel for applying the Canny edge detector. The edge gradient threshold then specifies the values of pixels to be taken as the edges and those remaining as

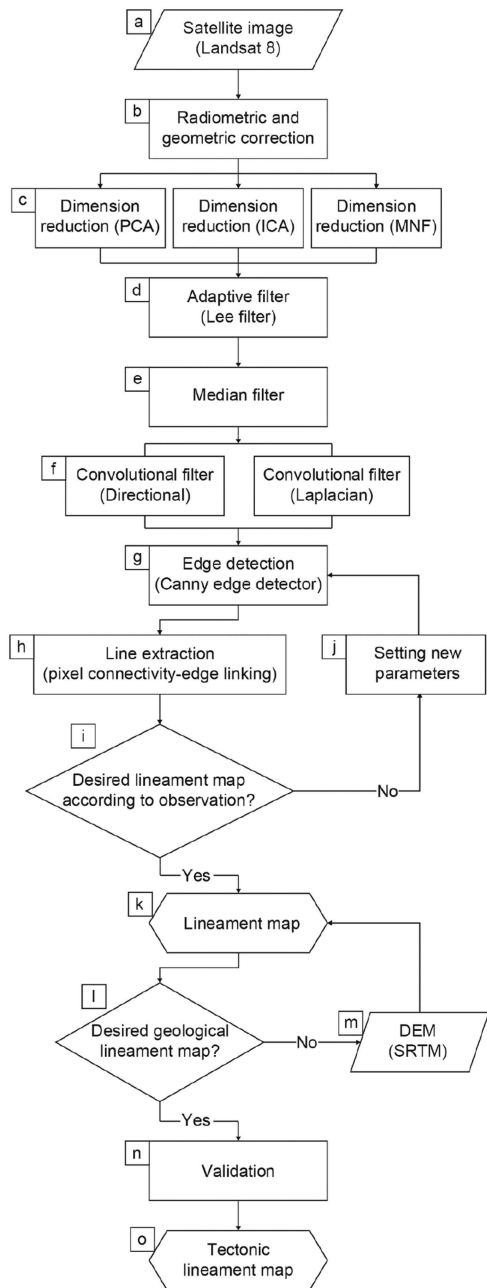


Figure 2. Methodology flowchart of this study for semi-automatic extraction of the tectonic lineaments. Input data to this flowchart include a digital satellite image (Landsat 8) and a digital elevation model (DEM). In this study, we use SRTM data as the input DEM.

background. Applying these two steps results in a binary map product. According to the curve length, this binary map undergoes a contour number reduction in order to leave just those referring to curves (Adiri et al. 2017). The resulting curves generate polylines if they fall within the tolerance defined by the line fitting error. Finally, two polylines in the simplest case will bind to form a lineament if their two end points form an angle

Table 1. Thresholds applied for the edge detection and line extraction in this study.

Threshold	Proposed range	Proposed value (directional filter)	Proposed value (Laplacian filter)
Filter radius (pixel)	3–8	5	5
Edge gradient	10–70	50	10
Curve length (pixel)	10–50	50	50
Line fitting error (pixel)	2–5	5	5
Angular difference (°)	3–20	10	10
Linking distance (pixel)	10–50	50	50

respecting the value specified by the angular difference and the distance by the linking distance (Adiri et al. 2017).

According to the spatial resolution of the OLI imagery, streams are the most important natural linear features which can be mistaken for tectonic linear features. Here, we used SRTM data with a spatial resolution of 30 m to delineate streams using the Esri Arc Hydro Tools (Figure 2(m)). The map of streams (Appendix B) is applied to convert a lineament map (Figure 2(k)) to a tectonic lineament map with minimal cultural and geomorphological lineaments (Figure 2(l,o)). A buffer zone with a radius of 5 pixels (150 m) surrounding the streams is created to prevent errors caused by shifting pixels in SRTM data. Lineaments that overlap the buffer zone by more than half their length are removed. Therefore, tectonic rather than cultural and geomorphological lineaments are more likely to be preserved in the final product (Figure 2(l,o)).

5. Results

5.1. Dimension reduction using MNF technique

The output component of the MNF with the highest eigenvalue (including polishing using Lee and median filters, Figure 2) yields a greyscale image shown in Figure 3. Tectonic lineaments are recognizable as dark and bright lines in the output component. Pixel values of the MNF component shows a positively skewed distribution and their range is small. According to the MNF component, dark and bright pixels as two anomalous populations of the pixel value distribution have been well separated. Please refer to Appendix A for more details on the comparison of dimension reduction techniques.

5.2. Directional and laplacian filters

Application of directional and Laplacian filters on the MNF component reveals natural and cultural lineaments (Figure 4). Streams and other large linear features can be readily identified in filtered images. However, there are some differences between the outputs of applying directional and Laplacian filters in terms of enhancing some of the tectonic lineaments. For example, the Laplacian filter failed to enhance most of the NW–SE striking tectonic lineaments located in the southwest of the study area, which are related to high number of hydrothermal mineral deposits. Applying a directional filter in different azimuths enhances geological structures striking in different directions and the results show that it is more robust in enhancing small lineaments compared to the Laplacian filter. Small NE–SW striking lineaments located in the northeast of the study area are probably

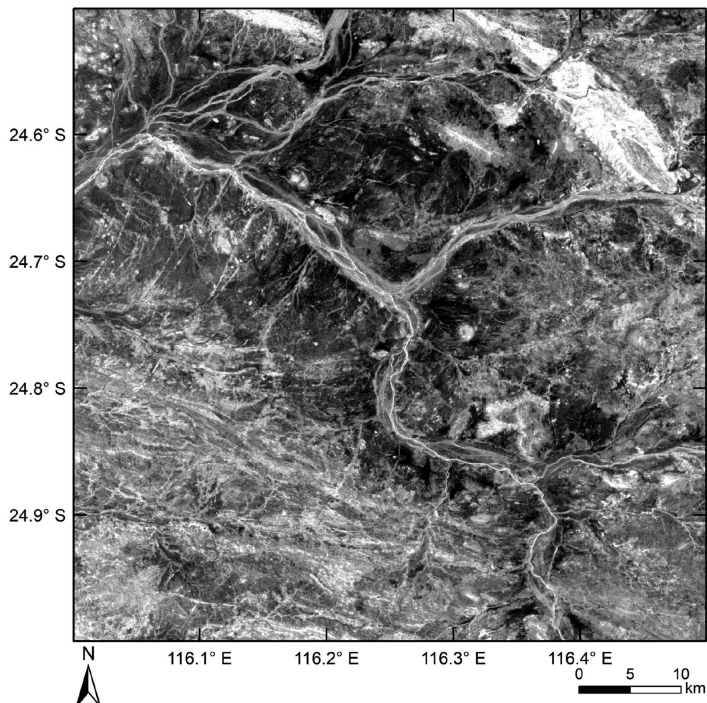


Figure 3. Greyscale image of the study area obtained by applying the MNF transformation.

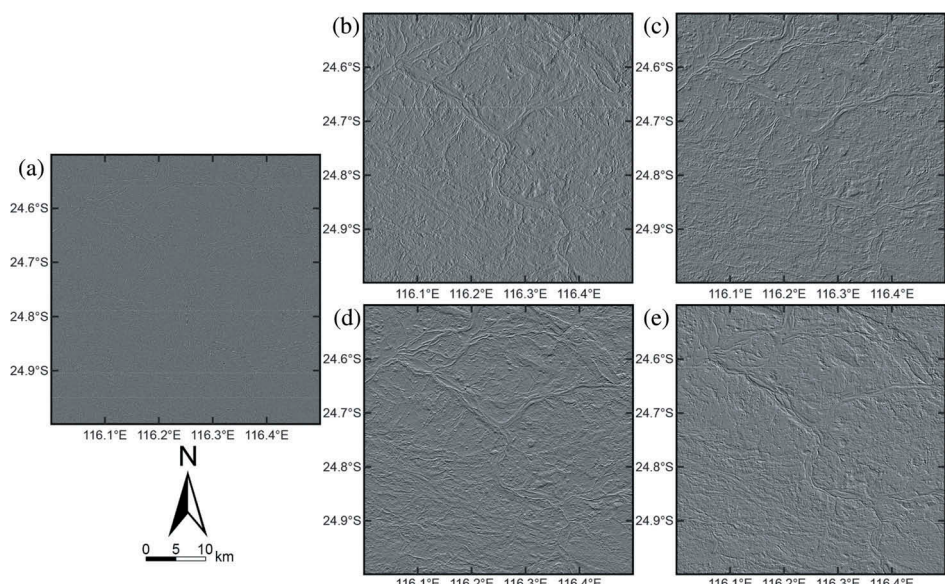


Figure 4. Images obtained by applying (a) a Laplacian filter and a directional filter in four directions with azimuths of (b) 0°, (c) 45°, (d) 90°, (e) 135° on the output component of the MNF technique with the highest eigenvalue.

mafic dykes (Mundine Well Dyke Swarm (Wingate and Giddings 2000)), and these are better enhanced using the directional filter compared to the Laplacian filter (Figure 4(a)).

5.3. Extraction of tectonic lineaments

The most recognizable natural linear features are streams, which may be mistaken for tectonic linear features (Appendix B). Removal of streams and their buffer zones yield different tectonic lineament maps for directional and Laplacian filters which are shown in Figure 5 draped over false colour composite image (Red Green Blue 752) of the study area. To aid visualization and validation, a lineament density map is produced for each of the filters as well as the GSWA lineament map to analyse the dispersion pattern of the lineaments (Figure 6).

The tectonic lineament map provided by the directional filter shows a significantly higher number of the lineaments compared to the map provided by the Laplacian filter (Figure 6). Comparison of these with the result of the GSWA map shows that the major trends of the tectonic lineaments have been displayed correctly. The map provided by the Laplacian filter is more correlated with the GSWA map but the density map of the tectonic lineaments extracted using the directional filter is highly correlated with hydrothermal mineral occurrences (Figure 6). Areas with high density values located in the northeast and southwest of the study area (Figure 6(b)) are associated with igneous granitic units, which can host diverse types of economic mineralization (Candela 1992).

5.4. Orientation analysis of extracted tectonic lineaments

The tectonic lineaments extracted via directional and Laplacian filters (Figure 5) reveal similar primary azimuth directions of 100° – 110° , which account for almost 10% and 12% of all extracted structures, respectively (Figures 6 and 7, Table 2). The directional and Laplacian filters show subtle differences in subordinate populations, striking at 20° – 30° and 40° – 50° , respectively (Figure 7, Table 2).

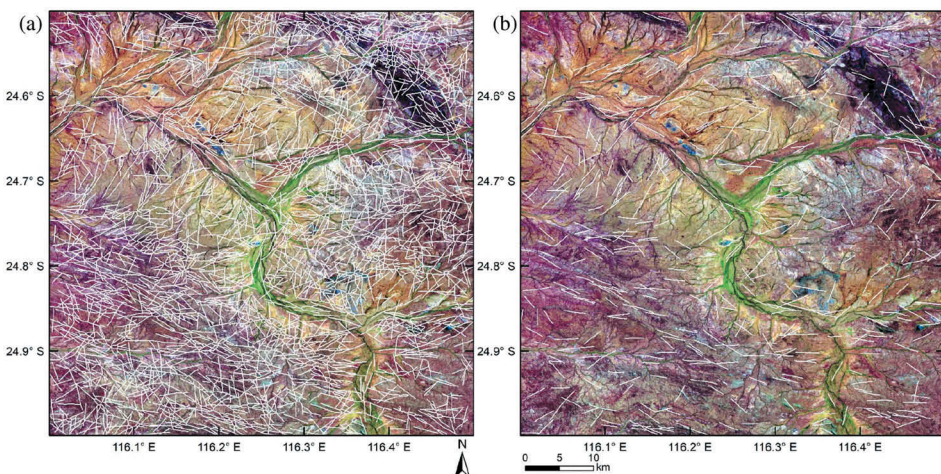


Figure 5. Extracted tectonic lineaments using the proposed framework and applying (a) directional, and (b) Laplacian filters.

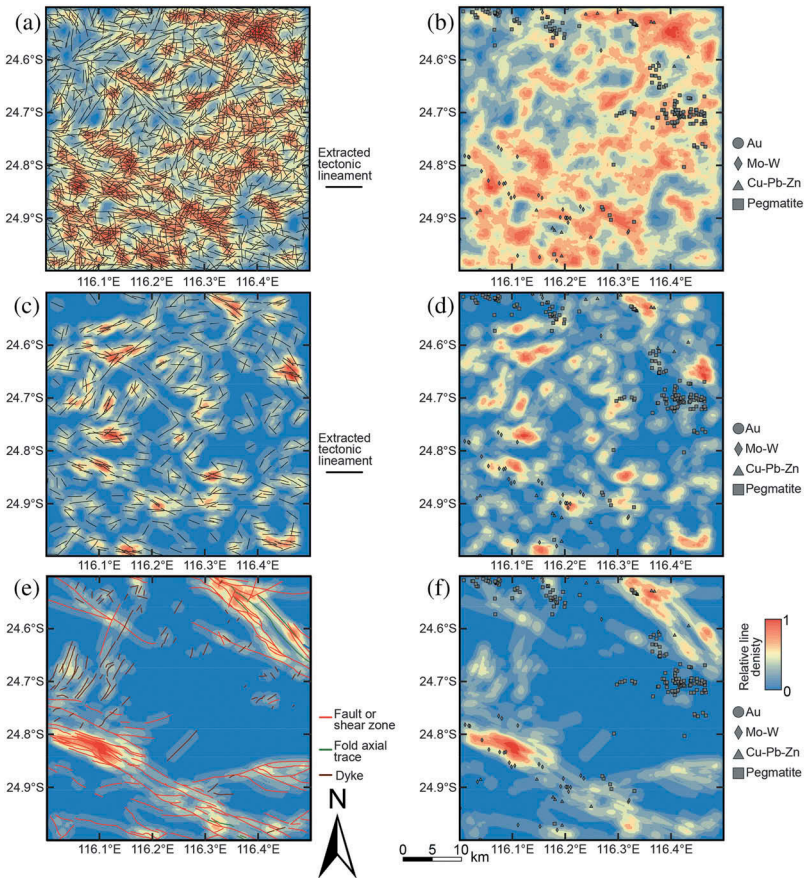


Figure 6. Superposition of tectonic lineaments and hydrothermal mineral occurrences on density maps resulted from the proposed framework using the MNF component improved by the (a), (b) directional and (c), (d) Laplacian filters; (e), (f) tectonic lineaments mapped by the GSWA. Density maps are created by summing the lineament length available in a defined grid size. For computational practicality, the size of each grid is set to 10 pixels (300 m) and the search radius is set to 50 pixels (1500 m). Lineament density values are taken into fuzzy space using a linear function, which yields values between 0 and 1 that makes it easier to compare them.

The NW–SE striking lineaments are strongly correlated with the GSWA map (Johnson et al. 2012, Figure 7). Geological mapping by the GSWA reveals a major azimuth of 110°–120° that accounts for almost 26% of all extracted tectonic lineaments (Figure 7(c), Table 2). There is a far broader spread of NW–SE trending structures for the extracted lineaments using remote sensing data compared to those mapped by the GSWA. The subordinate NE–SW striking features identified via semi-automated lineament extraction are comparatively rare in the GSWA map (Figures 6 and 7).

5.5. Correlation of tectonic lineaments with hydrothermal mineral occurrences

A strong spatial association is observed between tectonic lineaments (e.g. faults, dykes) and hydrothermal mineral occurrences. Converting tectonic lineaments into a density pattern (Figure 6) further supports the notion that tectonic lineaments and

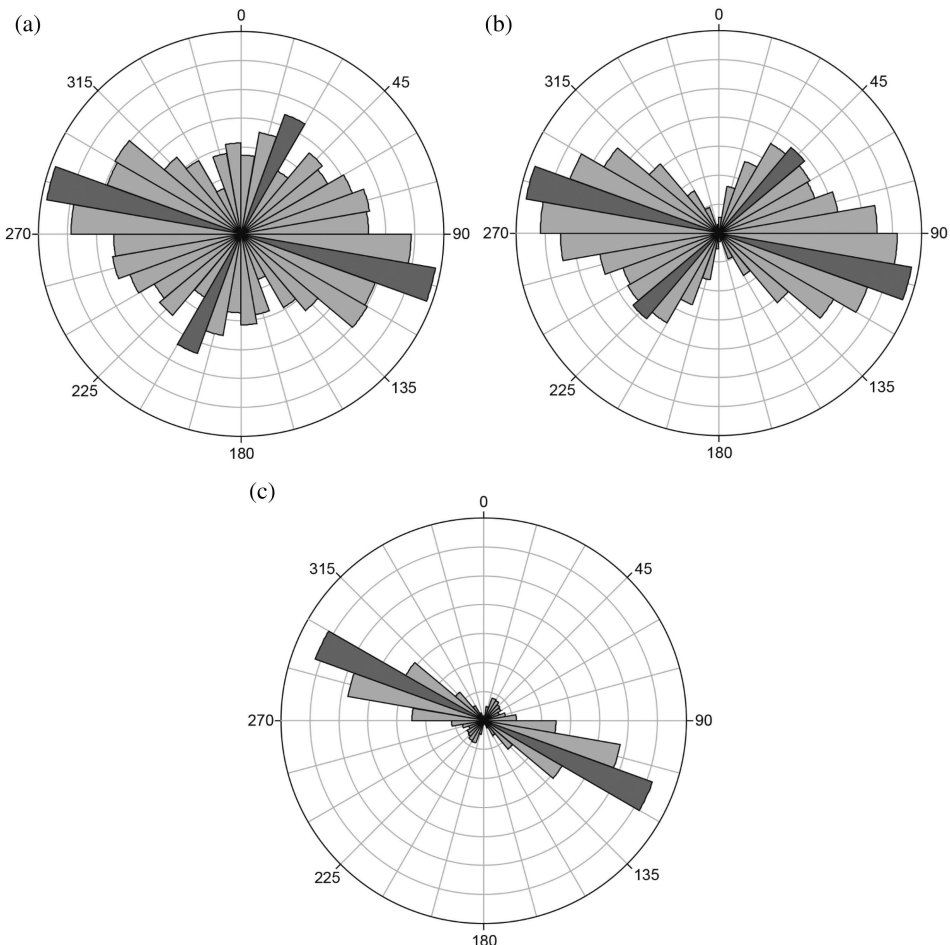


Figure 7. Rose diagrams showing the number and orientation of the tectonic lineaments extracted by the proposed framework using (a) directional and (b) Laplacian filters applied on the MNF component. As a means of validation, rose diagrams of the tectonic lineaments mapped by (c) the GSWA is also shown (S. P. Johnson et al. 2012).

hydrothermal mineralization are co-located. A density map of the extracted tectonic lineaments using a directional filter on the MNF component shows the highest correlation with hydrothermal occurrence locations (i.e. the highest area under curve in Figure 8). The result of applying a directional filter shows a better correlation with the hydrothermal mineralization compared to the GSWA lineament map which shows the lowest correlation with the hydrothermal mineral occurrences. Most of the extracted tectonic lineaments are located in Halfway Gneiss and Edmund Group in southwest and northeast of the study area, respectively. These units comprise meta-igneous felsic intrusive and sedimentary carbonate rocks. There is a high number of hydrothermal mineral occurrences in granitic units, while there are a few associated with the sedimentary units.

Table 2. Comparison of different tectonic lineament maps generated by applying different methods.

Method	Azimuth of the major strike	Frequency (%)	Azimuth of the minor strike	Frequency (%)
Proposed framework using directional filter	100–110	10	20–30	6
Proposed framework using Laplacian filter	100–110	12	40–50	6
GSWA tectonic lineament map	110–120	26	N/A	N/A

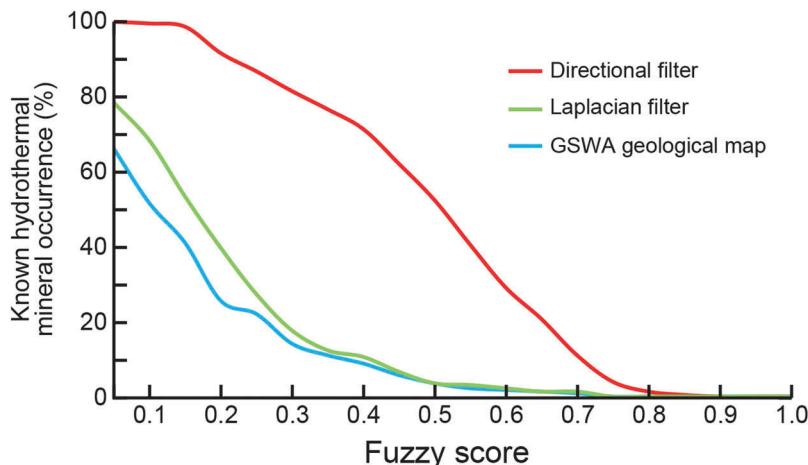


Figure 8. Spatial association between hydrothermal mineral occurrences and different tectonic lineament density maps. Lineament density values are taken into fuzzy space using a linear function. The x axis shows the fuzzy thresholds from 0 to 1. The y axis shows the percentage of known hydrothermal mineral occurrences that are placed in anomalous areas according to the thresholds shown in x axis.

6. Discussion

6.1. Evaluation of semi-automated computer vision framework

In general, evaluation and validation of the different operations used in this study, against geological mapping, reveals an optimum dimension reduction technique, convolutional filter and edge detection parameter values. Each of these processes are discussed in turn.

The geological mapping by the GSWA captured most, but not all of the tectonic lineaments in the Yinnetharra region of the Gascoyne Province (Johnson et al. 2012, Figure 6). Comparison of the extracted tectonic lineaments, using the proposed framework with the tectonic lineament map by the GSWA (Johnson et al. 2012), reveals that applying MNF dimension reduction transformation is a reliable technique and results are close to the field observations (Figure 3). The primary reason for the superior results from the MNF technique is high signal-to-noise ratio of the applied component (Vassilas et al. 2002; Nielsen 2011) and uniform behaviour of each pixel's brightness value (positive peaks) facing the tectonic lineaments.

Visual (Figure 6) and statistical (Figure 7) comparisons show that the extracted tectonic lineaments using the proposed framework and applying a Laplacian filter on the MNF

output component with the highest eigenvalue are well correlated with the GSWA tectonic lineament map. However, it is clear that the density map of the extracted tectonic lineaments using a directional filter is highly correlated with the hydrothermal mineral occurrences ([Figure 8](#)). The directional filter is able to enhance lineaments in desired directions which is an advantage in geological studies compared to the Laplacian filter. As geologists have prior knowledge of major structural trends, this approach is valid in regions where sufficient outcrop exists for field-based studies. Additionally, the images obtained by applying the directional filter significantly increases the efficiency of lineament extraction algorithms particularly through detecting small lineaments (Lopes et al. [2016](#)). The broader spread of extracted lineament data using both filters compared to those extracted using the GSWA map is attributed to the short length of the extracted tectonic lineaments ([Figure 7](#)) (Adiri et al. [2017](#)).

The Canny edge detection and pixel connectivity-edge linking algorithms have been widely used in different fields (Hashim et al. [2013](#); Ali and Clausi [2001](#); Liu and Jezek [2004](#); Elmahdy and Mohamed [2016](#)). In this study, we increased the efficiency of these methods for extracting tectonic lineaments using the proposed framework. The initial steps of the proposed framework including dimension reduction technique, adaptive and convolutional filters enhance the edges and increase the efficiency of edge detection and line extraction processes. Moreover, we present an optimum range of parameters applied in the lineament extraction operation for the Yinnetharra region ([Table 1](#)). Optimum values of mentioned parameters may be different for each study area because of different spectral characteristics in each region, but our values provide a baseline for future studies. According to the field observations and geological evidence such as hydrothermal mineral occurrences, which are highly correlated with the structural features, our proposed framework is able to extract a high fraction of the tectonic lineaments ([Figure 6](#)). Tectonic lineament density maps cannot be individually used for detecting hydrothermal mineral deposits, while a density map of the extracted tectonic lineaments using the proposed framework can be provided as the final product and can be used as an auxiliary evidential layer for detecting hydrothermal mineral deposits.

Tectonic lineament maps provided by field observations are biased by the mapping geologist, who may have different views in dealing with the same structural features. The proposed framework is significantly less biased by the operator, but it is possible to modify the final map by applying new parameters to approach the desired tectonic lineament map. Ultimately, although it is always important to validate results whenever possible to geological maps, additional lineaments may be revealed through a semi-automated computerized framework.

6.2. Limitations of the proposed framework and future improvements

The lineament extraction process applied in this study is limited to a specific curve length, while the tectonic lineaments show variable lengths on the Earth's surface. This semi-automated process extracts tectonic lineaments as multipart lines, which may be significantly in error with real structural discontinuities. Although structural discontinuities may naturally segmented by fault relays, longer, continuous faults are also likely to be present (Vermilye and Scholz [1999](#)). In terranes where regolith or sedimentary cover is a problem, it is often difficult to differentiate between linked and single faults and, consequently,

most geologists opt for producing single, longer faults as these require less inference (Taylor and Eggleton 2001; Fondriest et al. 2015). Applied edge detection and line extraction methods in the proposed framework can be replaced with recently introduced methods based on image segmentation for other applications, to overcome above mentioned limitations (Xiaoqi, Weixing, and Jun 2016).

The process of removing streams from the extracted lineaments using the proposed framework can also be improved by introducing new criteria through discriminating streams and tectonic lineaments. Here, an SRTM digital elevation model was used for mapping streams, but according to the Landsat 8 image (Figure 5), some bifurcated streams failed to be identified using our semi-automated framework. High resolution images obtained using unmanned aerial vehicle photogrammetry can be considered as alternative input data to the proposed framework to overcome limited spatial resolution of the satellite data for efficient discrimination of streams and tectonic lineaments (Vasuki et al. 2014). The input data to the proposed framework is limited to optical remote sensing data, but in addition to OLI, other data types such as enhanced thematic mapper plus (ETM+) and advanced spaceborne thermal emission and reflection (ASTER) data can be used for extracting tectonic lineaments.

Uncertainty is one of the most common challenges among the diverse areas of remote sensing. Voluminous data are being produced by various remote-sensing applications. However, sometimes it is not easy and possible to provide quantitative uncertainty information associated with the data to extract information and distill knowledge from the data. No geological map is ever flawless, but we considered mapping by the GSWA at a scale of 1:100,000 as an appropriate benchmark for assessing the validity of our final workflow results (Johnson et al. 2012). In future, new studies can be conducted on providing a method through quantifying the uncertainty of tectonic lineament extraction process.

The proposed framework can be considered as a general methodology, which can be also used in other geoscientific fields such as hydrogeological and tectonic studies for mapping tectonic lineaments. We emphasize that maps provided using the proposed framework, which show the exposed tectonic lineaments on the Earth's surface and deep-seated faults, can be further improved using other geophysical techniques, including magnetic, gravity and even radiometric data.

7. Conclusions

In this study, we present a computer vision-based framework for detecting tectonic lineaments using optical remote sensing data. The proposed framework involves diverse techniques for reducing dimensionality, removing noise and enhancing the lineaments in addition to edge detection and line extraction. The extracted tectonic lineaments using the output component of the MNF technique are well correlated with the available tectonic lineament map.

The Canny edge detector and pixel connectivity-edge linking algorithm are applied, respectively, to detect edges and to extract lines through providing a lineament map. The SRTM digital elevation model is applied to remove streams from the extracted lineaments to produce a tectonic lineament map. The extracted tectonic lineaments are compared to ground truth. Irrespective of the applied dimension reduction technique and convolutional

filter, we observe a high fraction of the extracted tectonic lineaments are matched to the GSWA tectonic lineament map.

We also investigate the correlation between the density map of the extracted tectonic lineaments and known hydrothermal mineral occurrences in the study area. We conclude that the tectonic lineaments which are extracted using a directional filter are highly correlated with the hydrothermal mineral occurrences. We demonstrate that the output of the proposed framework can be applied to create an efficient evidential layer for prospectivity mapping of the hydrothermal mineral deposits.

In future work, the proposed framework can be used to map tectonic lineaments in other regions using different kinds of optical remote sensing data acquired by other sensors. The incorporation of various sources of data such as other types of geophysical maps (e.g. gravity, magnetics, and radiometrics) can be used to further enhance the framework. Moreover, statistical methods can be used to optimize parameters applied in lineament extraction algorithms. This could lead to better the convergence of the rose diagram obtained from the extracted tectonic lineaments and the field observations which are close to the real data.

Acknowledgements

The authors would like to thank Prof. R. Singh for handling this paper. We also appreciate anonymous reviewers for their valuable comments which helped to improve this paper.

Disclosure statement

No potential conflict of interest was reported by the authors.

ORCID

Ehsan Farahbakhsh  <http://orcid.org/0000-0003-2618-2458>

References

- Adiri, Z., A. E. Harti, A. Jellouli, R. Lhissou, L. Maacha, M. Azmi, M. Zouhair, and E. M. Bachaoui. 2017. "Comparison of Landsat-8, ASTER and Sentinel 1 Satellite Remote Sensing Data in Automatic Lineaments Extraction: A Case Study of Sidi Flah-Bouskour Inlier, Moroccan Anti Atlas." *Advances in Space Research* 60 (11): 2355–2367. COSPAR. doi:[10.1016/j.asr.2017.09.006](https://doi.org/10.1016/j.asr.2017.09.006).
- Adiri, Z., A. E. Harti, A. Jellouli, L. Maacha, and E. M. Bachaoui. 2016. "Lithological Mapping Using Landsat 8 OLI and Terra ASTER Multispectral Data in the Bas Drâa Inlier, Moroccan Anti Atlas." *Journal of Applied Remote Sensing* 10 (1): 16005–16014. doi:[10.1111/j.1.JRS.10.016005](https://doi.org/10.1111/j.1.JRS.10.016005).
- Akinluyi, F. O., M. O. Olorunfemi, and O. G. Bayowa. 2018. "Investigation of the Influence of Lineaments, Lineament Intersections and Geology on Groundwater Yield in the Basement Complex Terrain of Ondo State, Southwestern Nigeria." *Applied Water Science* 8 (1): 49. doi:[10.1007/s13201-018-0686-x](https://doi.org/10.1007/s13201-018-0686-x).
- Ali, M., and D. Clausi. 2001. "Using the Canny Edge Detector for Feature Extraction and Enhancement of Remote Sensing Images." *IEEE International Geoscience and Remote Sensing Symposium* 5: 2298–2300. doi:[10.1109/IGARSS.2001.977981](https://doi.org/10.1109/IGARSS.2001.977981).

- Allibone, A., J. Teasdale, G. Cameron, M. Etheridge, P. Uttley, A. Soboh, J. Appiah-Kubi, et al. 2002. "Timing and Structural Controls on Gold Mineralization at the Bogoso Gold Mine, Ghana, West Africa." *Economic Geology* 97 (5): 949–969. doi:[10.2113/gsecongeo.97.5.949](https://doi.org/10.2113/gsecongeo.97.5.949).
- Arian, M., and R. Nouri. 2015. "Lineament Tectonics and Mineralizatin in Tarom Area, North Iran." *Open Journal of Geology* 5: 115–125. doi:[10.4236/ojg.2015.53011](https://doi.org/10.4236/ojg.2015.53011).
- Awad, A., and H. Man. 2008. "Similar Neighborhood Criterion for Edge Detection in Noisy and Noise-Free Images." In *International Multiconference on Computer Science and Information Technology*, 483–486. doi:[10.1109/IMCSIT.2008.4747287](https://doi.org/10.1109/IMCSIT.2008.4747287).
- Ballard, D. H., and C. M. Brown. 1982. *Computer Vision*. Englewood Cliffs, NJ: Prentice Hall.
- Beiranvand Pour, A., and M. Hashim. 2014. "Structural Geology Mapping Using PALSAR Data in the Bau Gold Mining District, Sarawak, Malaysia." *Advances in Space Research* 54 (4): 644–654. doi:[10.1016/j.asr.2014.02.012](https://doi.org/10.1016/j.asr.2014.02.012).
- Beiranvand Pour, A., and M. Hashim. 2015. "Structural Mapping Using PALSAR Data in the Central Gold Belt, Peninsular Malaysia." *Ore Geology Reviews* 64: 13–22. doi:[10.1016/j.oregeorev.2014.06.011](https://doi.org/10.1016/j.oregeorev.2014.06.011).
- Bhuiyan, C. 2015. "Hydrological Characterisation of Geological Lineaments: A Case Study from the Aravalli Terrain, India." *Hydrogeology Journal* 23 (4): 673–686. doi:[10.1007/s10040-015-1239-0](https://doi.org/10.1007/s10040-015-1239-0).
- Boardman, J. W., and F. A. Kruse. 1994. "Automated Spectral Analysis: A Geologic Example Using AVIRIS Data, North Grapevine Mountains, Nevada." In *10th Thematic Conference on Geologic Remote Sensing, Environmental Research Institute of Michigan*, 1407–1418.
- Candela, P. A. 1992. "Controls on Ore Metal Ratios in Granite-Related Ore Systems: An Experimental and Computational Approach." *Earth and Environmental Science Transactions of the Royal Society of Edinburgh* 83 (1–2): 317–326. Royal Society of Edinburgh Scotland Foundation. doi:[10.1017/S0263593300007999](https://doi.org/10.1017/S0263593300007999).
- Canny, J. 1986. "A Computational Approach to Edge Detection." *IEEE Transactions on Pattern Analysis and Machine Intelligence* 8 (6): 679–698. doi:[10.1109/TPAMI.1986.4767851](https://doi.org/10.1109/TPAMI.1986.4767851).
- Chan, R. H., H. Chung-Wa, and M. Nikolova. 2005. "Salt-And-Pepper Noise Removal by Median-Type Noise Detectors and Detail-Preserving Regularization." *IEEE Transactions on Image Processing* 14 (10): 1479–1485. doi:[10.1109/TIP.2005.852196](https://doi.org/10.1109/TIP.2005.852196).
- Cox, S. F. 1999. "Deformational Controls on the Dynamics of Fluid Flow in Mesothermal Gold Systems." *Geological Society, London, Special Publications* 155: 123–140. doi:[10.1144/GSL.SP.1999.155.01.10](https://doi.org/10.1144/GSL.SP.1999.155.01.10).
- Craw, D. 2000. "Fluid Flow at Fault Intersections in an Active Oblique Collision Zone, Southern Alps, New Zealand." *Journal of Geochemical Exploration* 69–70: 523–526. doi:[10.1016/S0375-6742\(00\)00094-7](https://doi.org/10.1016/S0375-6742(00)00094-7).
- Cross, A. M. 1988. "Detection of Circular Geological Features Using the Hough Transform." *International Journal of Remote Sensing* 9 (9): 1519–1528. Taylor & Francis. doi:[10.1080/01431168808954956](https://doi.org/10.1080/01431168808954956).
- Crow, W. T., and R. H. Reichle. 2008. "Comparison of Adaptive Filtering Techniques for Land Surface Data Assimilation." *Water Resources Research* 44(8). Wiley-Blackwell. doi:[10.1029/2008WR006883](https://doi.org/10.1029/2008WR006883).
- Cyganek, B. 2003. "Combined Detector of Locally-Oriented Structures and Corners in Images Based on a Scale-Space Tensor Representation of Local Neighborhoods of Pixels." In *International Conference on Computational Science*, edited by M. A. Peter, D. A. Sloot, A. V. Bogdanov, Y. E. Gorbachev, J. J. Dongarra, and A. Y. Zomaya, 721–730. Berlin, Heidelberg: Springer. doi:[10.1007/3-540-44862-4_78](https://doi.org/10.1007/3-540-44862-4_78).
- Daryani, N. J., M. Arian, and N. R. Omran. 2015. "Tectonics and Mineralisation of Copper in the Ardestan-Kahang Area, Central Iran by Remote Sensing." *Open Journal of Geology* 5 (4): 188–196. Scientific Research Publishing. doi:[10.4236/ojg.2015.54017](https://doi.org/10.4236/ojg.2015.54017).
- Dasho, O. A., E. A. Ariyibi, F. O. Akinluyi, M. O. Awoyemi, and A. S. Adebayo. 2017. "Application of Satellite Remote Sensing to Groundwater Potential Modeling in Ejigbo Area, Southwestern Nigeria." *Modeling Earth Systems and Environment* 3 (2): 615–633. doi:[10.1007/s40808-017-0322-z](https://doi.org/10.1007/s40808-017-0322-z).
- Dos Reis Salles, R., C. R. de Souza Filho, T. Cudahy, L. E. Vicente, and L. V. S. Monteiro. 2017. "Hyperspectral Remote Sensing Applied to Uranium Exploration: A Case Study at the Mary

- Kathleen Metamorphic-Hydrothermal U-REE Deposit, NW, Queensland, Australia." *Journal of Geochemical Exploration* 179: 36–50. doi:[10.1016/j.gexplo.2016.07.002](https://doi.org/10.1016/j.gexplo.2016.07.002).
- El Janati, M., A. Soulaimani, H. Admou, N. Youbi, A. Hafid, and K. P. Hefferan. 2014. "Application of ASTER Remote Sensing Data to Geological Mapping of Basement Domains in Arid Regions: A Case Study from the Central Anti-Atlas, Iguerda Inlier, Morocco." *Arabian Journal of Geosciences* 7 (6): 2407–2422. doi:[10.1007/s12517-013-0945-y](https://doi.org/10.1007/s12517-013-0945-y).
- Elmahdy, S. I., and M. M. Mohamed. 2016. "Mapping of Tecto-Lineaments and Investigate Their Association with Earthquakes in Egypt: A Hybrid Approach Using Remote Sensing Data." *Geomatics, Natural Hazards and Risk* 7 (2): 600–619. Taylor & Francis. doi:[10.1080/19475705.2014.996612](https://doi.org/10.1080/19475705.2014.996612).
- Fondriest, M., S. Aretusini, G. D. Toro, and S. A. F. Smith. 2015. "Fracturing and Rock Pulverization along an Exhumed Seismogenic Fault Zone in Dolostones: The Foiana Fault Zone (southern Alps, Italy)." *Tectonophysics* 654: 56–74. doi:[10.1016/j.tecto.2015.04.015](https://doi.org/10.1016/j.tecto.2015.04.015).
- Ghita, O., and P. F. Whelan. 2002. "Computational Approach for Edge Linking." *Journal of Electronic Imaging* 11 (4): 479–485. doi:[10.1117/1.1501574](https://doi.org/10.1117/1.1501574).
- Glasser, N. F., and M. C. Ghiglione. 2009. "Structural, Tectonic and Glaciological Controls on the Evolution of Fjord Landscapes." *Geomorphology* 105 (3): 291–302. doi:[10.1016/j.geomorph.2008.10.007](https://doi.org/10.1016/j.geomorph.2008.10.007).
- Green, A. A., M. Berman, P. Switzer, and M. D. Craig. 1988. "A Transformation for Ordering Multispectral Data in Terms of Image Quality with Implications for Noise Removal." *IEEE Transactions on Geoscience and Remote Sensing* 26 (1): 65–74. doi:[10.1109/36.3001](https://doi.org/10.1109/36.3001).
- Guru, D. S., B. H. Shekar, and P. Nagabhushan. 2004. "A Simple and Robust Line Detection Algorithm Based on Small Eigenvalue Analysis." *Pattern Recognition Letters* 25 (1): 1–13. doi:[10.1016/j.patrec.2003.08.007](https://doi.org/10.1016/j.patrec.2003.08.007).
- Gutierrez, S., and D. G. Long. 2002. "Computer Vision Applications to the Study of Sea-Ice Motion in Antarctica." *IEEE International Geoscience and Remote Sensing Symposium* 3: 1512–1514. doi:[10.1109/IGARSS.2002.1026165](https://doi.org/10.1109/IGARSS.2002.1026165).
- Hao, Q., X. Chen, N. Guoqiang, and H. Zhang. 2007. "Road and Linear Structure Automatic Extraction." In *Proceedings of SPIE - The International Society for Optical Engineering*. Vol. 6833. doi:[10.1117/12.757348](https://doi.org/10.1117/12.757348).
- Haralick, R. M., S. R. Sternberg, and X. Zhuang. 1987. "Image Analysis Using Mathematical Morphology." *IEEE Transactions on Pattern Analysis and Machine Intelligence* 9 (4): 532–550. doi:[10.1109/TPAMI.1987.4767941](https://doi.org/10.1109/TPAMI.1987.4767941).
- Harris, J. R., D. Rogge, R. Hitchcock, O. Ijewliw, and D. Wright. 2005. "Mapping Lithology in Canada's Arctic: Application of Hyperspectral Data Using the Minimum Noise Fraction Transformation and Matched Filtering." *Canadian Journal of Earth Sciences* 42 (12): 2173–2193. NRC Research Press. doi:[10.1139/e05-064](https://doi.org/10.1139/e05-064).
- Hashim, M., S. Ahmad, M. A. M. Johari, and A. B. Pour. 2013. "Automatic Lineament Extraction in a Heavily Vegetated Region Using Landsat Enhanced Thematic Mapper (ETM+) Imagery." *Advances in Space Research* 51 (5): 874–890. doi:[10.1016/j.asr.2012.10.004](https://doi.org/10.1016/j.asr.2012.10.004).
- He, Y., F. Wang, Q. Wu, and Q. Wang. 2008. "Change Patterns of Linear Features in Remote Sensing Images in Land Use." *Transactions of the Chinese Society of Agricultural Engineering* 24 (12): 111–115. doi:[10.3969/j.issn.1002-6819.2008.12.023](https://doi.org/10.3969/j.issn.1002-6819.2008.12.023).
- Hein, J. R., K. Mizell, A. Koschinsky, and T. A. Conrad. 2013. "Deep-ocean Mineral Deposits as a Source of Critical Metals for High- and Green-Technology Applications: Comparison with Land-Based Resources." *Ore Geology Reviews* 51: 1–14. doi:[10.1016/j.oregeorev.2012.12.001](https://doi.org/10.1016/j.oregeorev.2012.12.001).
- Hewson, R., D. Robson, A. Carlton, and P. Gilmore. 2017. "Geological Application of ASTER Remote Sensing within Sparsely Outcropping Terrain, Central New South Wales, Australia." *Cogent Geoscience* 3(1). Cogent. doi:[10.1080/23312041.2017.1319259](https://doi.org/10.1080/23312041.2017.1319259).
- Huang, X., L. Zhang, and P. Li. 2007. "Classification and Extraction of Spatial Features in Urban Areas Using High-Resolution Multispectral Imagery." *IEEE Geoscience and Remote Sensing Letters* 4 (2): 260–264. doi:[10.1109/LGRS.2006.890540](https://doi.org/10.1109/LGRS.2006.890540).
- Irons, J. R., J. L. Dwyer, and J. A. Barsi. 2012. "The Next Landsat Satellite: The Landsat Data Continuity Mission." *Remote Sensing of Environment* 122: 11–21. doi:[10.1016/j.rse.2011.08.026](https://doi.org/10.1016/j.rse.2011.08.026).

- James, M. R., and S. Robson. 2012. "Straightforward Reconstruction of 3D Surfaces and Topography with a Camera: Accuracy and Geoscience Application." *Journal of Geophysical Research: Earth Surface* 117 (F3): n/a-n/a. Wiley-Blackwell. doi:10.1029/2011JF002289.
- Johnson, S. P., F. J. Korhonen, C. L. Kirkland, J. B. Cliff, E. A. Belousova, and S. Sheppard. 2017. "An Isotopic Perspective on Growth and Differentiation of Proterozoic Orogenic Crust: From Subduction Magmatism to Cratonization." *Lithos* 268–271: 76–86. doi:10.1016/j.lithos.2016.11.003.
- Johnson, S. P., S. Sheppard, P. B. Groenewold, and T. R. Farrell. 2012. "Yinnetharra, WA Sheet 2148, 1:100000 Geological Series." *Geological Survey of Western Australia*. <http://www.dmp.wa.gov.au/Geological-Survey/Geology-of-Western-Australia-1389.aspx>
- Johnson, S. P., S. Sheppard, B. Rasmussen, M. T. D. Wingate, C. L. Kirkland, J. R. Muhling, I. R. Fletcher, and E. A. Belousova. 2011. "Two Collisions, Two Sutures: Punctuated Pre-1950Ma Assembly of the West Australian Craton during the Ophthalmian and Glenburgh Orogenies." *Precambrian Research* 189 (3): 239–262. doi:10.1016/j.precamres.2011.07.011.
- Johnson, S. P., A. M. Thorne, I. M. Tyler, R. J. Korsch, B. L. N. Kennett, H. N. Cutten, J. Goodwin, et al. 2013. "Crustal Architecture of the Capricorn Orogen, Western Australia and Associated Metallogeny." *Australian Journal of Earth Sciences* 60 (6–7): 681–705. Taylor & Francis. doi:10.1080/08120099.2013.826735.
- Karantzalos, K., and D. Argialas. 2006. "Improving Edge Detection and Watershed Segmentation with Anisotropic Diffusion and Morphological Levellings." *International Journal of Remote Sensing* 27 (24): 5427–5434. Taylor & Francis. doi:10.1080/01431160600944010.
- Karnieli, A., A. Meisels, L. Fisher, and Y. Arkin. 1996. "Automatic Extraction and Evaluation of Geological Linear Features from Digital Remote Sensing Data Using a Hough Transform." *Photogrammetric Engineering and Remote Sensing* 62 (5): 525–531. American Society of Photogrammetry.
- Korhonen, F. J., S. P. Johnson, M. T. D. Wingate, C. L. Kirkland, I. R. Fletcher, D. J. Dunkley, M. P. Roberts, S. Sheppard, J. R. Muhling, and B. Rasmussen. 2017. "Radiogenic Heating and Craton-margin Plate Stresses as Drivers for Intraplate Orogeny." *Journal of Metamorphic Geology* 35 (6): 631–661. Wiley/Blackwell (10.1111/jmg.12249).
- Krapež, B., S. G. Müller, I. R. Fletcher, and B. Rasmussen. 2017. "A Tale of Two Basins? Stratigraphy and Detrital Zircon Provenance of the Palaeoproterozoic Turee Creek and Horseshoe Basins of Western Australia." *Precambrian Research* 294: 67–90. doi:10.1016/j.precamres.2017.03.020.
- Lafon, S., and A. B. Lee. 2006. "Diffusion Maps and Coarse-Graining: A Unified Framework for Dimensionality Reduction, Graph Partitioning, and Data Set Parameterization." *IEEE Transactions on Pattern Analysis and Machine Intelligence* 28 (9): 1393–1403. doi:10.1109/TPAMI.2006.184.
- Lageson, D. R. 2009. *Introduction to Field Mapping of Geologic Structures*. Bozeman, MT: Montana State University.
- Lee, J. S. 1980. "Digital Image Enhancement and Noise Filtering by Use of Local Statistics." *IEEE Transactions on Pattern Analysis and Machine Intelligence* 2 (2): 165–168. doi:10.1109/TPAMI.1980.4766994.
- Lee, Y. H., and S. Y. Park. 1990. "A Study of Convex/Concave Edges and Edge-Enhancing Operators Based on the Laplacian." *IEEE Transactions on Circuits and Systems* 37 (7): 940–946. doi:10.1109/31.55069.
- Lisle, R. J. 2003. *Geological Structures and Maps; A Practical Guide*. Three. Butterworth-Heinemann. doi:10.1016/B978-075065780-8/50002-1.
- Liu, H., and K. C. Jezek. 2004. "Automated Extraction of Coastline from Satellite Imagery by Integrating Canny Edge Detection and Locally Adaptive Thresholding Methods." *International Journal of Remote Sensing* 25 (5): 937–958. Taylor & Francis. doi:10.1080/0143116031000139890.
- Lopes, F. C., A. J. Pereira, V. M. Mantas, and H. K. Mpengo. 2016. "Morphostructural Characterization of the Western Edge of the Huila Plateau (SW Angola), Based on Remote Sensing Techniques." *Journal of African Earth Sciences* 117: 114–123. doi:10.1016/j.jafrearsci.2016.01.007.
- Loveland, T. R., and J. L. Dwyer. 2012. "Landsat: Building a Strong Future." *Remote Sensing of Environment* 122: 22–29. doi:10.1016/j.rse.2011.09.022.

- Lu, Y., L. Liu, and X. Guojian. 2016. "Constraints of Deep Crustal Structures on Large Deposits in the Cloncurry District, Australia: Evidence from Spatial Analysis." *Ore Geology Reviews* 79: 316–331. doi:[10.1016/j.oregeorev.2016.05.022](https://doi.org/10.1016/j.oregeorev.2016.05.022).
- Lund, K., R. G. Tysdal, K. V. Evans, M. J. Kunk, and R. M. Pillers. 2011. "Structural Controls and Evolution of Gold-, Silver-, and REE-Bearing Copper-Cobalt Ore Deposits, Blackbird District, East-Central Idaho: Epigenetic Origins." *Economic Geology* 106 (4): 585–618. doi:[10.2113/econgeo.106.4.585](https://doi.org/10.2113/econgeo.106.4.585).
- Manuel, R. D., M. Brito, M. Chichorro, and C. Rosa. 2017. "Remote Sensing for Mineral Exploration in Central Portugal." *Minerals* 7 (10): 184. doi:[10.3390/min7100184](https://doi.org/10.3390/min7100184).
- Marghan, M., and M. Hashim. 2010. "Lineament Mapping Using Multispectral Remote Sensing Satellite Data." *International Journal of the Physical Sciences* 5 (10): 1501–1507. doi:[10.3923/rijasci.2010.126.130](https://doi.org/10.3923/rijasci.2010.126.130).
- Martinez, J. M., J. L. Guyot, N. Filizola, and F. Sondag. 2009. "Increase in Suspended Sediment Discharge of the Amazon River Assessed by Monitoring Network and Satellite Data." *CATENA* 79 (3): 257–264. doi:[10.1016/j.catena.2009.05.011](https://doi.org/10.1016/j.catena.2009.05.011).
- Masoud, A., and K. Koike. 2006. "Tectonic Architecture through Landsat-7 ETM+/SRTM DEM-Derived Lineaments and Relationship to the Hydrogeologic Setting in Siwa Region, NW Egypt." *Journal of African Earth Sciences* 45 (4–5): 467–477. doi:[10.1016/j.jafrearsci.2006.04.005](https://doi.org/10.1016/j.jafrearsci.2006.04.005).
- Masoud, A., and K. Koike. 2017. "Applicability of Computer-Aided Comprehensive Tool (LINDA: LINEament Detection and Analysis) and Shaded Digital Elevation Model for Characterizing and Interpreting Morphotectonic Features from Lineaments." *Computers & Geosciences* 106: 89–100. Elsevier. doi:[10.1016/j.cageo.2017.06.006](https://doi.org/10.1016/j.cageo.2017.06.006).
- Masoud, A. A., and K. Koike. 2011. "Auto-Detection and Integration of Tectonically Significant Lineaments from SRTM DEM and Remotely-Sensed Geophysical Data." *ISPRS Journal of Photogrammetry and Remote Sensing* 66 (6): 818–832. International Society for Photogrammetry and Remote Sensing, Inc. (ISPRS). doi:[10.1016/j.isprsjprs.2011.08.003](https://doi.org/10.1016/j.isprsjprs.2011.08.003).
- Nath, B., Z. Niu, and A. K. Mitra. 2019. "Observation of Short-Term Variations in the Clay Minerals Ratio after the 2015 Chile Great Earthquake (8.3 Mw) Using Landsat 8 OLI Data." *Journal of Earth System Science* 128 (5): 117. doi:[10.1007/s12040-019-1129-2](https://doi.org/10.1007/s12040-019-1129-2).
- Nath, B., Z. Niu, and S. Acharjee. 2017. "Pre-Earthquake Anomaly Detection and Assessment through Lineament Changes Observation Using Multi-Temporal Landsat 8-OLI Imageries: Case of Gorkha and Imphal." In *Multi-Purposeful Application of Geospatial Data*. doi:[10.5772/intechopen.72735](https://doi.org/10.5772/intechopen.72735).
- Nielsen, A. A. 2011. "Kernel Maximum Autocorrelation Factor and Minimum Noise Fraction Transformations." *IEEE Transactions on Image Processing* 20 (3): 612–624. doi:[10.1109/TIP.2010.2076296](https://doi.org/10.1109/TIP.2010.2076296).
- Olierook, H. K. H., A. Agangi, D. Plavsa, S. M. Reddy, W. Yao, C. Clark, S. A. Occhipinti, and A. R. C. Kylander-Clark. 2019a. "Neoproterozoic Hydrothermal Activity in the West Australian Craton Related to Rodinia Assembly or Breakup?" *Gondwana Research* 68: 1–12. doi:[10.1016/j.gr.2018.10.019](https://doi.org/10.1016/j.gr.2018.10.019).
- Olierook, H. K. H., S. P. Stephen Sheppard, S. A. Johnson, S. M. Occhipinti, C. C. Reddy, I. R. Fletcher, et al. 2018. "Extensional Episodes in the Paleoproterozoic Capricorn Orogen, Western Australia, Revealed by Petrogenesis and Geochronology of Mafic–Ultramafic Rocks." *Precambrian Research* 306: 22–40. doi:[10.1016/j.precamres.2017.12.015](https://doi.org/10.1016/j.precamres.2017.12.015).
- Olierook, H. K. H., R. J. M. Taylor, T. M. Erickson, C. Clark, S. M. Reddy, C. L. Kirkland, I. Jahn, and M. Barham. 2019b. "Unravelling Complex Geologic Histories Using U–Pb and Trace Element Systematics of Titanite." *Chemical Geology* 504: 105–122. doi:[10.1016/j.chemgeo.2018.11.004](https://doi.org/10.1016/j.chemgeo.2018.11.004).
- Paiva, R. C. D., M. T. Durand, and F. Hossain. 2015. "Spatiotemporal Interpolation of Discharge across a River Network by Using Synthetic SWOT Satellite Data." *Water Resources Research* 51 (1): 430–449. Wiley-Blackwell. doi:[10.1002/2014WR015618](https://doi.org/10.1002/2014WR015618).
- Patel, A. K., and S. Chatterjee. 2016. "Computer Vision-Based Limestone Rock-Type Classification Using Probabilistic Neural Network." *Geoscience Frontiers* 7 (1): 53–60. doi:[10.1016/j.gsf.2014.10.005](https://doi.org/10.1016/j.gsf.2014.10.005).
- Patel, J., J. Patwardhan, K. Sankhe, and R. Kumbhare. 2011. "Fuzzy Inference Based Edge Detection System Using Sobel and Laplacian of Gaussian Operators." In *International Conference & Workshop on Emerging Trends in Technology*, 694–697. ACM. doi:[10.1145/1980022.1980171](https://doi.org/10.1145/1980022.1980171).

- Petrov, V. A., Y. L. Rebetsky, V. V. Poluektov, and A. A. Burmistrov. 2015. "Tectonophysics of Hydrothermal Ore Formation: An Example of the Antei Mo–U Deposit, Transbaikalia." *Geology of Ore Deposits* 57 (4): 292–312. doi:[10.1134/S1075701515040030](https://doi.org/10.1134/S1075701515040030).
- Piechocka, A. M., C. J. Gregory, Z. Jian-Wei, M. T. Stephen Sheppard, D. Wingate, and B. Rasmussen. 2017. "Monazite Trumps Zircon: Applying SHRIMP U-Pb Geochronology to Systematically Evaluate Emplacement Ages of Leucocratic, Low-Temperature Granites in a Complex Precambrian Orogen." *Contributions to Mineralogy and Petrology* 172 (8): 63. doi:[10.1007/s00410-017-1386-5](https://doi.org/10.1007/s00410-017-1386-5).
- Piechocka, A. M., I. C. Stephen Sheppard, W. Fitzsimons, S. P. Johnson, B. Rasmussen, and F. Jourdan. 2018. "Neoproterozoic 40Ar/39Ar Mica Ages Mark the Termination of a Billion Years of Intraplate Reworking in the Capricorn Orogen, Western Australia." *Precambrian Research* 310: 391–406. doi:[10.1016/j.precamres.2018.04.006](https://doi.org/10.1016/j.precamres.2018.04.006).
- Pirajno, F. 2004. "Metallogeny in the Capricorn Orogen, Western Australia, the Result of Multiple Ore-Forming Processes." *Precambrian Research* 128 (3): 411–439. doi:[10.1016/j.precamres.2003.09.010](https://doi.org/10.1016/j.precamres.2003.09.010).
- Pirasteh, S., B. Pradhan, H. O. Safari, and M. F. Ramli. 2013. "Coupling of DEM and Remote-Sensing-Based Approaches for Semi-Automated Detection of Regional Geostructural Features in Zagros Mountain, Iran." *Arabian Journal of Geosciences* 6 (1): 91–99. doi:[10.1007/s12517-011-0361-0](https://doi.org/10.1007/s12517-011-0361-0).
- Pour, B., H. M. Amin, M. Charles, and Z. Khin. 2016. "Structural Mapping of the Bentong-Raub Suture Zone Using PALSAR Remote Sensing Data, Peninsular Malaysia: Implications for Sediment-hosted/Orogenic Gold Mineral Systems Exploration." *Resource Geology* 66 (4): 368–385. Wiley/Blackwell. doi:[10.1111/rge.12105](https://doi.org/10.1111/rge.12105).
- Raharimahefa, T., and T. M. Kusky. 2009. "Structural and Remote Sensing Analysis of the Betsimisaraka Suture in Northeastern Madagascar." *Gondwana Research* 15 (1): 14–27. doi:[10.1016/j.gr.2008.07.004](https://doi.org/10.1016/j.gr.2008.07.004).
- Rahnama, M., and R. Gloaguen. 2014a. "TecLines: A MATLAB-Based Toolbox for Tectonic Lineament Analysis from Satellite Images and DEMs, Part 1: Line Segment Detection and Extraction." *Remote Sensing* 6 (7): 5938–5958. doi:[10.3390/rs61111468](https://doi.org/10.3390/rs61111468).
- Rahnama, M., and R. Gloaguen. 2014b. "TecLines: A MATLAB-Based Toolbox for Tectonic Lineament Analysis from Satellite Images and DEMs, Part 2: Line Segments Linking and Merging." *Remote Sensing* 6 (11): 11468–11493. doi:[10.3390/rs61111468](https://doi.org/10.3390/rs61111468).
- Ramli, M. F., N. Yusof, M. K. Yusoff, H. Juahir, and H. Z. M. Shafri. 2010. "Lineament Mapping and Its Application in Landslide Hazard Assessment: A Review." *Bulletin of Engineering Geology and the Environment* 69 (2): 215–233. doi:[10.1007/s10064-009-0255-5](https://doi.org/10.1007/s10064-009-0255-5).
- Rasmussen, B., I. R. Fletcher, and S. Sheppard. 2005. "Isotopic Dating of the Migration of a Low-Grade Metamorphic Front during Orogenesis." *Geology* 33 (10): 773–776. doi:[10.1130/G21666.1](https://doi.org/10.1130/G21666.1).
- Reuter, D., C. Richardson, J. Irons, R. Allen, M. Anderson, J. Budinoff, G. Casto, et al. 2010. "The Thermal Infrared Sensor on the Landsat Data Continuity Mission." In *IEEE International Geoscience and Remote Sensing Symposium*, 754–757. doi:[10.1109/IGARSS.2010.5653746](https://doi.org/10.1109/IGARSS.2010.5653746).
- Richards, J. A. 2013. *Remote Sensing Digital Image Analysis: An Introduction*. 5th ed. Springer. doi:[10.1007/978-3-642-30062-2](https://doi.org/10.1007/978-3-642-30062-2).
- Saad, A. Z. E., and Z. Mohammed. 2011. "Contribution of the Interpretation of ETM+ Satellite Images to the Analysis of the Fracturation of the Tifrit Mole Region of Saïda." In *Recent Advances in Environment, Energy Systems and Naval Science: Proceedings of the 4th International Conference on Environmental and Geological Science and Engineering*, Barcelona, Spain, 246–257.
- Saadi, N., and K. Watanabe. 2008. "Lineaments Extraction and Analysis in Eljufra Area, Libya." *Journal of Applied Remote Sensing* 2 (1): 23516–23538. doi:[10.1117/1.2994727](https://doi.org/10.1117/1.2994727).
- Saadi, N. M., E. Aboud, and K. Watanabe. 2009. "Integration of DEM, ETM+, Geologic, and Magnetic Data for Geological Investigations in the Jifara Plain, Libya." *IEEE Transactions on Geoscience and Remote Sensing* 47 (10): 3389–3398. doi:[10.1109/TGRS.2009.2020911](https://doi.org/10.1109/TGRS.2009.2020911).
- Shahzad, F., and R. Gloaguen. 2011. "TecDEM: A MATLAB Based Toolbox for Tectonic Geomorphology, Part 1: Drainage Network Preprocessing and Stream Profile Analysis." *Computers & Geosciences* 37 (2): 250–260. doi:[10.1016/j.cageo.2010.06.008](https://doi.org/10.1016/j.cageo.2010.06.008).

- Sheppard, S., S. Bodorkos, S. P. Johnson, M. T. D. Wingate, and C. L. Kirkland. 2010. "The Paleoproterozoic Capricorn Orogeny: Intracontinental Reworking Not Continent–Continent Collision." *GSPA Record* 108: 1–33.
- Sheppard, S., S. A. Occhipinti, and D. R. Nelson. 2005. "Intracontinental Reworking in the Capricorn Orogen, Western Australia: The 1680 – 1620 Ma Mangaroon Orogen*." *Australian Journal of Earth Sciences* 52 (3): 443–460. Taylor & Francis. doi:[10.1080/08120090500134589](https://doi.org/10.1080/08120090500134589).
- Sheppard, S., B. Rasmussen, J. R. Muhling, T. R. Farrell, and I. R. Fletcher. 2007. "Grenvillian-aged Orogenesis in the Palaeoproterozoic Gascoyne Complex, Western Australia: 1030–950 Ma Reworking of the Proterozoic Capricorn Orogen." *Journal of Metamorphic Geology* 25 (4): 477–494. Wiley/Blackwell. doi:[10.1111/j.1525-1314.2007.00708.x](https://doi.org/10.1111/j.1525-1314.2007.00708.x).
- Simonet, D. S., and F. T. Ulaby. 1983. *Manual of Remote Sensing-Volume I: Theory, Instruments and Techniques*. Falls Church, VA: American Society of Photogrammetry.
- Singh, P. P., and R. D. Garg. 2013. "Automatic Road Extraction from High Resolution Satellite Image Using Adaptive Global Thresholding and Morphological Operations." *Journal of the Indian Society of Remote Sensing* 41 (3): 631–640. doi:[10.1007/s12524-012-0241-4](https://doi.org/10.1007/s12524-012-0241-4).
- Singh, R. P., A. K. Sanjeeb Bhoi, U. R. Sahoo, and S. Ravindranath. 2001. "Surface Manifestations after the Gujarat Earthquake." *Current Science* 81 (2): 164–166. JSTOR.
- Singh, V. P., and R. P. Singh. 2005. "Changes in Stress Pattern around Epicentral Region of Bhuj Earthquake of 26 January 2001." *Geophysical Research Letters* 32 (24). doi:[10.1029/2005GL023912](https://doi.org/10.1029/2005GL023912).
- Sonka, M., V. Hlavac, and R. Boyle. 2014. *Image Processing, Analysis, and Machine Vision*. 4th ed. Boston, MA: Cengage Learning.
- Szeliski, R. 2010. *Computer Vision: Algorithms and Applications*. London, UK: Springer.
- Takorabt, M., A. C. Toubal, H. Haddoum, and S. Zerrouk. 2018. "Determining the Role of Lineaments in Underground Hydrodynamics Using Landsat 7 ETM+ Data, Case of the Chott El Gharbi Basin (western Algeria)." *Arabian Journal of Geosciences* 11 (4): 76. doi:[10.1007/s12517-018-3412-y](https://doi.org/10.1007/s12517-018-3412-y).
- Taylor, G., and R. A. Eggleton. 2001. *Regolith Geology and Geomorphology*. John Wiley & Sons.
- Thenkabail, P. S., P. G. Teluguntla, M. K. Gumma, and V. Dheeravath. 2015. "Hyperspectral Remote Sensing for Terrestrial Applications." Chap. 9 in *Remote Sensing Handbook (Volume II): Land Resources Monitoring, Modeling, and Mapping with Remote Sensing* 201–233. CRC.
- Tripathi, N. K., K. V. G. K. Gokhale, and M. U. Siddiqui. 2000. "Directional Morphological Image Transforms for Lineament Extraction from Remotely Sensed Images." *International Journal of Remote Sensing* 21 (17): 3281–3292. doi:[10.1080/014311600750019895](https://doi.org/10.1080/014311600750019895).
- US Geological Survey. 2019. "EarthExplorer." <https://earthexplorer.usgs.gov>
- Valero, S., J. Chanussot, J. A. Benediktsson, H. Talbot, and B. Waske. 2010. "Advanced Directional Mathematical Morphology for the Detection of the Road Network in Very High Resolution Remote Sensing Images." *Pattern Recognition Letters* 31 (10): 1120–1127. doi:[10.1016/j.patrec.2009.12.018](https://doi.org/10.1016/j.patrec.2009.12.018).
- van der Werff, H., and V. D. M. Freek. 2016. "Sentinel-2A MSI and Landsat 8 OLI Provide Data Continuity for Geological Remote Sensing." *Remote Sensing* 8 (11): 883. doi:[10.3390/rs8110883](https://doi.org/10.3390/rs8110883).
- Vassilas, N., S. Perantonis, E. Charou, T. Tsenoglou, M. Stefouli, and S. Varoufakis. 2002. "Delineation of Lineaments from Satellite Data Based on Efficient Neural Network and Pattern Recognition Techniques." In *2nd Hellenic Conference on AI : Methods and Applications of Artificial Intelligence*, Thessaloniki, Greece.
- Vasuki, Y., E.-J. Holden, P. Kovesi, and S. Micklethwaite. 2014. "Semi-automatic Mapping of Geological Structures Using UAV-Based Photogrammetric Data: An Image Analysis Approach." *Computers & Geosciences* 69: 22–32. doi:[10.1016/j.cageo.2014.04.012](https://doi.org/10.1016/j.cageo.2014.04.012).
- Vermilye, J. M., and C. H. Scholz. 1999. "Fault Propagation and Segmentation: Insight from the Microstructural Examination of a Small Fault." *Journal of Structural Geology* 21 (11): 1623–1636. doi:[10.1016/S0191-8141\(99\)00093-0](https://doi.org/10.1016/S0191-8141(99)00093-0).
- Vučinić, P., Ž. Trpovski, and I. Šćepan. 2010. "Automatic Landmarking of Cephalograms Using Active Appearance Models." *European Journal of Orthodontics* 32 (3): 233–241. doi:[10.1093/ejo/cjp099](https://doi.org/10.1093/ejo/cjp099).
- Wang, J. 1993. "Linda — A System for Automated Linear Feature Detection and Analysis." *Canadian Journal of Remote Sensing* 19 (1): 9–21. doi:[10.1080/07038992.1993.10855146](https://doi.org/10.1080/07038992.1993.10855146).

- Wingate, M. T. D., and J. W. Giddings. 2000. "Age and Palaeomagnetism of the Mundine Well Dyke Swarm, Western Australia: Implications for an Australia–Laurentia Connection at 755 Ma." *Precambrian Research* 100 (1): 335–357. doi:[10.1016/S0301-9268\(99\)00080-7](https://doi.org/10.1016/S0301-9268(99)00080-7).
- Xiaoqi, L., W. Weixing, and L. Jun. 2016. "A Method of Road Extraction from High-Resolution Remote Sensing Images Based on Shape Features." *Acta Geodaetica Et Cartographica Sinica* 38 (5): 457–465. Directory of Open Access Journals.
- Yang, K., S. Sam Ge, and H. He. 2011. "Robust Line Detection Using Two-Orthogonal Direction Image Scanning." *Computer Vision and Image Understanding* 115 (8): 1207–1222. doi:[10.1016/j.cviu.2011.03.010](https://doi.org/10.1016/j.cviu.2011.03.010).
- Zhang, K., and J. T. Kwok. 2010. "Clustered Nystrom Method for Large Scale Manifold Learning and Dimension Reduction." *IEEE Transactions on Neural Networks* 21 (10): 1576–1587. doi:[10.1109/TNN.2010.2064786](https://doi.org/10.1109/TNN.2010.2064786).
- Zhang, L., J. Wu, T. Hao, and J. Wang. 2006. "Automatic Lineament Extraction from Potential-Field Images Using the Radon Transform and Gradient Calculation." *Geophysics* 71 (3): 31–40. doi:[10.1190/1.2194521](https://doi.org/10.1190/1.2194521).
- Zhang, L., and W. Xiaolin. 2006. "An Edge-Guided Image Interpolation Algorithm via Directional Filtering and Data Fusion." *IEEE Transactions on Image Processing* 15 (8): 2226–2238. doi:[10.1109/TIP.2006.877407](https://doi.org/10.1109/TIP.2006.877407).
- Zi, J.-W., B. Rasmussen, J. R. Muhling, I. R. Fletcher, A. M. Thorne, S. P. Johnson, H. N. Cutten, D. J. Dunkley, and F. J. Korhonen. 2015. "In Situ U–Pb Geochronology of Xenotime and Monazite from the Abra Polymetallic Deposit in the Capricorn Orogen, Australia: Dating Hydrothermal Mineralization and Fluid Flow in a Long-Lived Crustal Structure." *Precambrian Research* 260: 91–112. doi:[10.1016/j.precamres.2015.01.010](https://doi.org/10.1016/j.precamres.2015.01.010).

Appendix A. Comparison of dimension reduction techniques

The efficiency of three dimension reduction techniques are compared in terms of enhancing the lineaments. The output component of the PCA, ICA and MNF with the highest eigenvalue (including polishing using Lee and median filters on each, [Figure 2](#)) yields greyscale images presented in [Figure A1](#). Tectonic lineaments are recognizable as dark and bright lines in the three output components ([Figure A1](#)). Pixel values of the PCA and ICA components show negatively skewed distributions, while the MNF component shows a positively skewed distribution. The range of pixel values in the PCA component is much higher than the ICA and MNF components. Comparison of the components shows that dark and bright pixels as two anomalous populations of the pixel value distribution have been better separated in the MNF component.

Comparison of the different dimension reduction techniques with manual photointerpretation shows that the MNF component is more robust than the PCA and ICA components for extracting tectonic lineaments ([Figure A2](#)). Focusing on a horizontal profile across a small sector in the west of

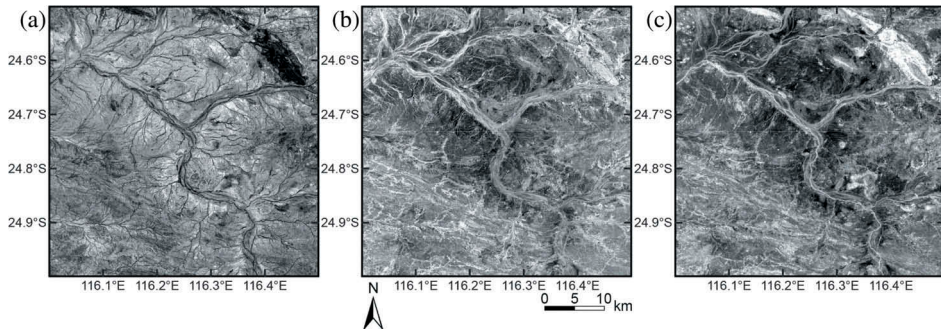


Figure A1. Output components of the (a) PCA, (b) ICA and (c) MNF techniques with the highest eigenvalue. These components have been polished by the Lee and median filters respectively.

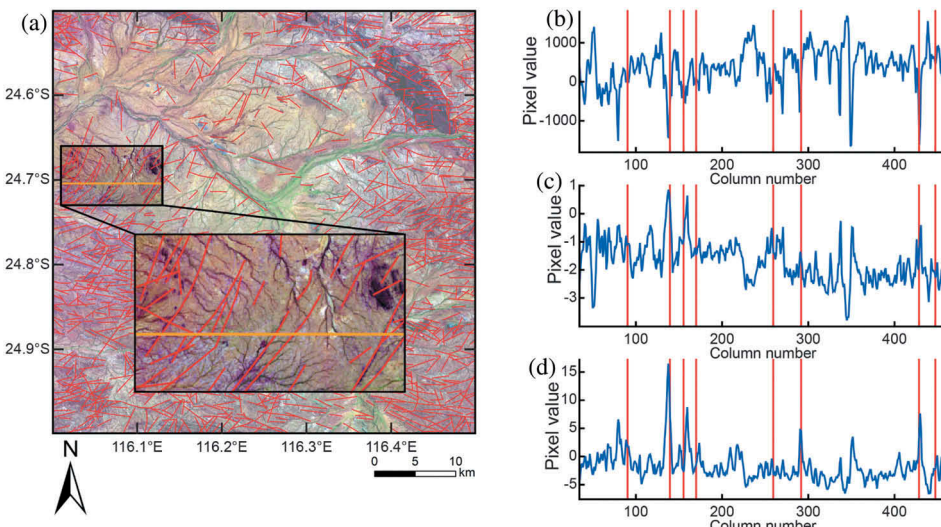


Figure A2. (a) Tectonic lineament map provided by manual photointerpretation draped over a false Landsat 8 colour composite image (Red Green Blue 752). The investigated horizontal profile in this map is shown in orange. (b) – (d) The changes of pixel values relevant to the PCA, ICA and MNF components with the highest eigenvalue across the profile, respectively.

the Yinnetharra map sheet reveals that the number of peaks (i.e. positive anomalous pixels) on the profile obtained from the MNF component correlates well with the intersected tectonic lineaments identified via manual photointerpretation. The MNF profile shows a relatively uniform background signal with strongly pronounced positive anomalies. In contrast, the graphs obtained from the PCA and ICA components show intense fluctuation across the profile, showing a poorer correlation to the lineaments identified via manual photointerpretation.

Appendix B. Map of streams

We used SRTM data with a spatial resolution of 30 m to delineate streams using the Esri Arc Hydro Tools. The map of streams ([Figure A3](#)) is applied to convert a lineament map to a tectonic lineament map with minimal cultural and geomorphological lineaments.

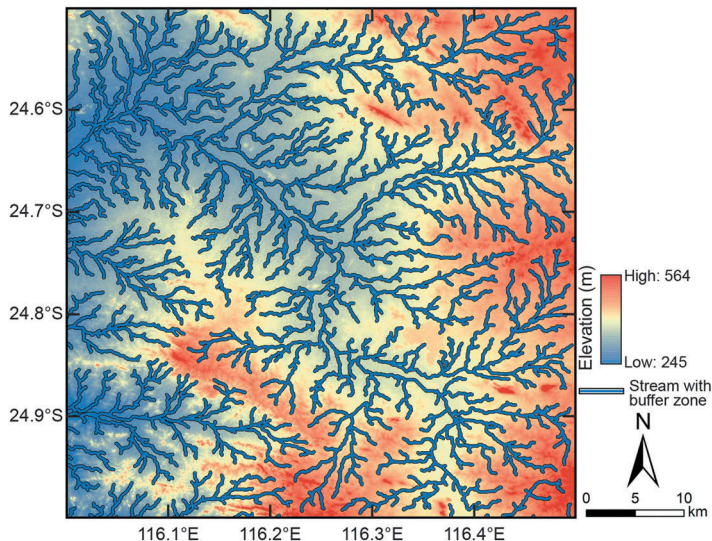


Figure A3. Extracted streams using SRTM data.